Desalination and Water Treatment
www.deswater.com

doi: 10.5004/dwt.2018.22814

126 (2018) 97–115
September

Combined linear Fresnel solar Rankine cycle with multi-effect desalination (MED) process: effect of solar DNI level on the electricity and water production costs

Ighball Baniasad Askari[a,*], Mehran Ameri[b]

[a]*Department of Mechanical Engineering, Faculty of Engineering, University of Zabol, Sistan & Baluchestan, P.O. Box 98615-538, Iran, Tel. +(98) 54-31232020; email: eghball.baniasad@uoz.ac.ir*
[b]*Department of Mechanical Engineering, Faculty of Engineering, Shahid Bahonar University of Kerman, P.O. Box 76175-133, Kerman, Iran, Tel. +(98) 34-22111763; email: ameri_mm@mail.uk.ac.ir*

Received 22 January 2018; Accepted 21 July 2018

ABSTRACT

In the present study, the direct steam generated from a linear Fresnel solar field was considered to be used as the working fluid of a Rankine cycle. Four regions located in North and South hemispheres and with different annual direct normal irradiance levels, ranging from 1,950 to 2,750 kWh/m^2, were selected to investigate the effect of solar radiation on the performance of a linear Fresnel/solar Rankine cycle (LF/SRC). The condenser of the LF/SRC plant was considered to be replaced by a multi-effect desalination (MED) unit. Different thermal storage capacities were considered for the LF/SRC plant with the electricity generation and water production rates of 85 MW and 80,000 m^3/d, respectively. Not only the required solar field area, thermal energy storage (TES) capacity, solar multiple (SM) were investigated but also the water and electricity costs of the plant. A sensitivity analysis was performed on solar field cost, TES system cost and fuel cost in order to determine the sensitivity of the electricity and water unit of costs to each of the mentioned cost parameters. In order to determine the effect of plant size on the water and electricity unit of costs, the calculations were made for the SRC/MED/LF plant with the larger scales.

Keywords: MED; Linear Fresnel; Solar Rankine cycle; Thermal storage; Natural gas boiler; DNI

1. Introduction

The application of the solar thermal power to produce the electricity and fresh water is a promising technology which leads to a significant reduction in fuel energy consumption. The water and energy scarcity in the regions such as Middle East and North Africa (MENA) countries is one of the major challenges and it is of importance for the researchers and investigators nowadays. The most important desalination processes driven by thermal energy are multistage flash (MSF) and multi-effect distillation (MED), which the later needs low energy consumptions as compared with the former. Despite the advances in energy efficiency during the last decade, seawater desalination continues to be an intensive fossil energy consumer. The MED is more efficient as compare with MSF and reverse osmosis (RO) because of its longer operation life, lower capital cost and lower pumping power [1]. The integration of the concentrating solar power (CSP) plants with the MED desalination units is becoming an alternative to solve the water crisis. Several research studies have been done on the combination of solar thermal technologies and desalination plants [2,3] as well as the performance of the solar organic Rankine cycles (SORC) [4,5]. The following literature review describes part of the previous research works on the CSP technology:

* Corresponding author.

1.1. CSP/electricity

Qoaider and Liqreina [6] investigated the effectiveness of dry cooled CSP plants in hot arid regions (the Middle East and North Africa (MENA)). In that research, the improvements of the performance of dry cooled CSP plants in the MENA region was investigated by optimizing their design configurations and adapting them for local conditions. The results show that the plants with oversized solar field (solar multiple of 2) and large thermal energy storage (TES) systems (8 h of thermal storage) perform better and can generate power at lower costs than smaller plants. The electricity generation costs were obtained as a value between 0.12 and 0.13 €/kWh for dry cooled power plants.

Three different solar power plants (photovoltaic [PV], CSP and PV/CSP) with the same electricity generation rate of 50 MW were investigated by Parrado et al. [7]. The results of that study have shown that the PV/CSP plant is a feasible option to contribute to the continuous delivery of sustainable electricity in Northern Chile. The electricity generation costs of the CSP, PV and hybrid CSP/PV plants were found to be as 0.15, 0.11 and 0.14 $/kWh, respectively. Also, it was shown that the electricity generation cost of the three described plants will be reduced to 0.077 $/kWh for the year of 2015.

The future economics of the CSP plants for Egypt was investigated by Shouman and Khattab [8]. A road map strategy was presented to remove the main barriers for financing and starting market introduction in the peak load and the medium load segment of power supply. For the calculation of cost development of CSP in the future, the expectations for the CSP capacity expansion were considered to be from 2,900 to 29,000 MW by 2015, from 20,000 to 150,000 MW by 2020, from 230,000 to 340,000 MW by 2030, and from 850,000 to 1,500,000 MW by 2050. The results of that study show that the CSP electricity generation cost is roughly equal to 0.28 $/kWh for 2010; which will be decreased to 0.08 $/kWh by 2050.

The application of the PTC and linear Fresnel (LF) solar fields as the thermal source of an SORC power generation plant with 1 MWe electricity generation rate was investigated by Cocco and Cau [9]. Different SM values and thermal storage capacities were considered to evaluate the performance of two CSP solutions. The results of that study show that the LF/SORC plants have higher values of the electrical energy production rates per unit area of the occupied land area (50–60 kWh/m^2/year) as compared with the PTC/SORC plants (45–55 kWh/m^2/year). The SM corresponding to the minimum levelized cost of electricity (LCOE) of the SORC plant, with 8 h of thermal storage, was found to be as 2.1 and 2.6 for PTC and LF solar fields, respectively.

Balghouthi et al. [10] investigated the potentials of solar resources in Tunisia. The authors presented the suitable factors for the deployment of the CSP plants in that country. The simulations of a PTC-based SRC power plant with the electricity generation rate of 50 MW were performed based on the solar radiation and climatic data delivered by the installed station. The results of that study show that the CSP project becomes economically competitive in Tunisia when the majority of the plant components such as the collectors structure, the mirrors and the storages system would be manufactured locally in Tunisia. The PTC solar field total required area was obtained as 510,120 m^2 with the total investment costs of €261,250,000 and the electricity generation cost of 0.23 €/kWh.

Another development in the power generation sector is the integration of CSP plants with the gas turbine power plants [11–16]. As it has been proven, the integrated solar combined cycle (ISCC) power plants allow reducing the LCOE of solar generated electricity by 35%–40% relative to the stand-alone CSP plants. Technical and economic feasibility of integrating CSP technologies with cogeneration gas turbine systems have been investigated by Mokheimer et al. [17]. In that work, three CSP technologies of solar tower, parabolic trough collector (PTC) and linear Fresnel reflector (LFR) were assessed for possible integration with a gas turbine cogeneration system that generates steam at a constant flow rate. A thermo-economic comparative analysis was conducted for all possible configurations of the integrated solar gas turbine cogeneration plant to find the optimal configurations based on the levelized electricity cost (LEC). The simulation results of that work show that the optimal configuration is the integration of LFR with the steam side of a gas turbine cogeneration plant with the LEC of 0.05 US$/kWh.

Two ISCC power plants based on PTC and LFR technologies were investigated by Rovira et al. [18]. The PTC and LFR solar fields were considered to be integrated with a high pressure level heat recovery steam generator. The results of that work revealed that the proposed evaporative configurations increase the annual performance. Also, it was found that the application of the PTC solar field entails higher thermal contribution; however, the LFR may improve the economic feasibility of the plant.

1.2. CSP/electricity/desalination

The SRC/MED and SRC/RO dual purpose (electricity/desalination) plants were investigated by Fichtner and DLR [19] for Mediterranean Sea, Atlantic Ocean, Red Sea and Persian Gulf. The water and electricity costs of both plants with water production capacity of 100,000 m^3/d were determined for the locations with different annual solar radiation levels of 2,000; 2,400 and 2,800 kWh/m^2/year. The electricity costs of the plants were found to be a value between 0.2 and 0.24 $/kWh with the corresponding water production costs of ranging from 1.6 to 1.9 $/m^3.

A thermo economic analysis of dual purpose (SRC/MED and SRC/RO) CSP plants was carried out by Ortega-Delgado et al. [20]. Direct steam generated from a PTC solar field was considered to be used as the thermal source of the CSP plant having the electricity generation rate of 5 MW. Two water desalination technologies of MED and RO were considered to be coupled with the CSP plant when it is located in Almeria, Spain. Four scenarios were investigated in that study; the MED replacing the condenser of the power block (PB), the MED being fed by the extracted steam from the PB, the RO directly uses the electricity generated in the PB, and the RO connected to the local grid. The minimum electricity cost was found for the RO unit connected to the local electricity grid.

Water desalination technologies and their possible coupling with CSP and PV electricity power were evaluated by Fiorenza et al. [21]. In that study, the MED and RO plants with different water production capacities ranging from 500 to 5,000 m^3/d were investigated and the economic results

were compared with the results obtained for a conventional desalination system. The water production costs for the plant with capacity of 5,000 m^3/d was found as 2.05, 2 and 0.85 \$/m^3 for PV/RO, CSP/MED and conventional plants, respectively.

The SRC/RO and SRC/MED plants were investigated by Palenzuela et al. [22]. In the SRC/MED plant, the MED unit was considered to be used as the condenser of a PTC-based SRC plant. The solar land improvement cost, solar field cost, heat transfer fluid (HTF) system cost, and the TES system cost were considered as 15 \$/m^3, 150 \$/m^3, 90 \$/m^3 and 35 \$/kWht, respectively, in the economic analysis of that work. The water production rate of 36,000 m^3/d was considered for that CSP plant with the electricity generation rate of 55 MW. The water production costs of the SRC/MED and SRC/RO configurations were found to be as 0.91 and 1 \$/m^3, respectively, for the solar thermal energy contribution of 54%.

The annual performance of the SRC/MED plants was investigated by Bataineh [23]. The study area was Aqaba which is located in a coastal region Jordan. The plant performance was investigated under different operating and geometrical conditions. The required solar field aperture area and thermal storage size of the CSP/MED plant were determined to produce 50,000 m^3 of fresh water per day.

A thermo-exergic analysis on the SORC plant having a thermal storage system was performed by Sharaf et al. [24]. In that research, the direct steam generated by the PTC solar field was considered to be used as the motive steam of the MED/TVC (thermal vapor compressions) system. Also, an MED/MVC (mechanical vapor compression) desalination unit was considered to be fed using the output steam extracted from the high pressure turbine of the SORC plant. The water production costs of the MED/TVC and MED/MVC desalination plants were determined as 1.5 and 2.1 \$/m^3, respectively, for the water production rate of 4,545 m^3/d.

A parametric study of a MED/TVC plant coupling with a Rankine cycle power block was conducted by Ortega-Delgado et al. [25]. In that work, a mathematical model of the MED/TVC system was developed in order to investigate the effect of the motive and suction steam pressures on the gain output ratio (GOR), fresh water production, the specific heat transfer area and other key variables. The research work emphasizes rather on the optimum characteristics of the MED/TVC plant than the Rankine cycle operational condition.

Single RO and hybrid MED/RO desalination systems integrated with both SRC and the conventional steam plants were considered by Moser et al. [26] under different fuel price scenarios. The water production cost for hybrid MED/RO (with 12 effects of MED) and single RO units were obtained as 0.85 and 0.8 \$/m^3, respectively, for the conventional power plant with the fuel price scenario of 0.8 \$/barrel. Also, the water production costs were obtained as 1.22 and 1.10 \$/m^3 for the hybrid SRC/MED/RO (with 12 effects of MED) and SRC/RO units, respectively.

The integration of the MED plant to a supercritical CO_2 Brayton cycle was investigated by Kouta et al. [27]. The solar power tower with a thermal storage system was used as the thermal source of the Brayton cycles and the MED plant. In that study, a cost analysis was performed for different regions in Saudi Arabia, and the findings show that the regions with the high annual solar irradiation level have the low LCOE and levelized cost of water (LCOW) values. The LCOE and LCOW of the described system were determined for different solar fractions. The results of that study show that, for the solar fraction of 0.5, the LCOE of the system varies between 0.09 and 0.11 \$/kWh, and also the system LCOW ranges between 0.9 and 1.15 \$/m^3.

The combination of the SRC plants with MED and RO desalination systems was investigated by Iaquaniello et al. [28]. The required thermal power of the MED unit was considered to be supplied using the exhaust steam delivered from the back pressure steam turbine of the plant. Also, part of the required electricity of the RO unit was considered to be supplied by the electricity generated from the same steam turbine and the other part was considered to be supported by a conventional gas turbine. Two different life times of 20 and 30 years were considered for the SRC/MED and SRC/RO systems in the economic analysis of that study. The results of that research show that increasing the system lifetime from 20 to 30 years would result in 8.8% decrease in the water production cost.

A dynamic simulation model of a novel solar–geothermal polygeneration system and the related exergetic and exergoeconomic analyses was performed by Calise et al. [29]. An organic Rankine cycle (ORC) plant was designed to supply the fresh water, electricity, heating and cooling requirements of a small community. The required thermal energy of the ORC plant was considered to be supplied by using a medium-enthalpy geothermal thermal energy source and also a PTC solar field. The geothermal fluid was considered to supply the required heat of a MED unit. The results of that study have shown that the exergoeconomic costs of the electricity, chilled water, cooling water and desalinated water vary, respectively, in the ranges of 0.1475–0.1722 €/kWh, 0.1863–0.1888 €/kWh_{ex}, 0.01612–0.01702 €/kWh_{ex} and 0.5695–0.6023 €/kWh_{ex}.

Sharaf et al. [30] used two techniques in order to investigate the MED system integrated with the SORC. In the first one, the solar output thermal energy is directly utilized to the first effect of the MED process via evaporator of a heat exchanger. In the second technique, the exhausted energy from the SORC steam turbine was considered to be used in the first effect of the MED process. Different MED configurations of parallel feed (PF), forward feed (FF) and backward feed (BF) were considered in that study. The water production costs for the first and second techniques were obtained as 1.62 and 1.87 \$/m^3, respectively, for the system with the water capacity of 5,000 m^3/d. The low water capacity rate of the 100 m^3/d was shown to have the higher water production costs range from 5.47 to 13.75 \$/m^3 for different MED configurations.

The application of linear Fresnel (LF) solar fields as the thermal source of the MED/TVC desalination process was investigated by Askari and Ameri [31] for the MED/TVC water production capacity of 9,000 m^3/d. Two LF solar fields were considered in that work; one of which was assumed to be used as the thermal source of the MED/TVC plant during the day time and the other one was considered to store the solar thermal energy and to use that during the night hours. The water production cost was determined for the system with different thermal storage capacities and also different areas of the LF solar field. The results of that study show that the water production cost of the MED/TVC/LF system is obtained as a value between 1.63 and 3.09 \$/m^3 for the

systems without thermal storage and with thermal storage, respectively.

LF has several advantages such as less sensitivity to wind, light weight reflector, more standard components, low land use, having the gaps to reduce shading/blocking effects, flexible choice of HTF. Also, LF could be applied for both direct steam generation and direct molten salt. LF design allows efficiency improvement [32,33] and reduced acquisition costs [34]. In the LFRs technology, the collector width and focal length could be designed up to 20 and 30 m, respectively. LFRs have a fix receiver and capture 55%–65% of the direct normal irradiance (DNI). This concentrator has low performance on the sun rise/set and high at noon. The maximum theoretical concentration and optical efficiency of LFRs is lower than PTCs. However, the use of stationary receiver without rotating joints or high-temperature moving components makes LFRs safer and more cost-effective than PTCs [35].

Previous research studies mainly focused on the PTC solar field as the thermal source of the SRC or SORC plants. As it can be derived from the previous literatures, no considerable research work has been conducted on the integration of the MED desalination unit with a LF/SRC plant. Also, the effect of DNI level on the electricity and water costs of the described system has not been considered in the previous studies. The LF technology requires lower land area and its initial capital investment is lower than the PTC solar field. Besides, the direct steam generated from the LF solar field can be used as the working fluid of the Rankine Cycle, whereas the PTC solar field with the steam HTF cannot operate under the high pressures, since the synthetic oils are usually used as the HTF in the PTC solar field. In the PTC-based SRCs, the thermal energy of the solar field HTF is transferred to the Rankine cycle HTF (steam) by using a heat exchanger, since part of the solar thermal energy is wasted through this operation. The application of the LF solar field as the thermal energy source of the dual purpose (electricity/water) plants can reduce the electricity generation and water production costs of the plants. Also, the LF technology is suitable for the locations with limited land areas.

In the previous research works, one PTC solar field has been considered to supply the required thermal energy of the Rankine cycle and also to charge the TES system using the PTC extra solar thermal power. This strategy does not allow the TES system to be charged under the temperatures higher than the Rankine cycle oil-steam heat exchanger required top temperature. In order to simplify the control strategy of the TES system operational conditions, two LF solar fields were considered in this paper; each one can operate at different temperatures. Therefore, it will become possible to have different output temperatures and various amounts of output thermal power for the two solar fields at the same time. The present study was carried out to estimate the water and electricity cost of the LF/SRC/MED system when it is located in any location around the world with different DNI level. The water steam was considered as the HTF of the solar field and the Rankine cycle. Also, the required solar field area and the percentage of the solar share for different thermal storage capacities are determined for the locations with different solar radiation levels.

The solar radiation data of four regions located in Iran, United Arab Emirates (UAE), Chile and Australia were used in the present work in order to consider the effect of solar DNI on the electricity generation and water production costs of the SRC/MED/LF plant. The specifications of a typical MED desalination plant with the GOR of 12 were used in the calculations of the present work. The main objectives were to find the solar multiples, percentage of the solar share and the electricity generation and water production costs of the SRC/MED/LF plant for different solar thermal storage capacities when it is located in four locations of the study. The effect of the plant scale on water production and electricity generation costs was also considered in the present work.

2. Study areas

Five years (2007–2011) hourly solar radiation data and ambient dry bulb temperature of the Kish Island was collected from the Iran Meteorological Organization [36] to be used in the calculations. For the other three locations, the system advisor model (SAM) software hourly solar radiation data were used in the calculations [37]. The described data are the International Weather for Energy Calculation weather data for the time period of (1982–1999), which included DNI, diffuse radiation, dry and wet bulb temperatures as well as wind speed and wind directions of three regions of the study. The total annual DNI and the time period of the weather data for four locations of the study are shown in Table 1.

2.1. Port Hedland

Port Hedland (20.18°S, 118.36°E) is the second largest town in the Pilbara region of Western Australia, with a population of approximately 14,000; including the town of South Hedland. The major resource activities supported by the town include the offshore natural gas fields, salt, manganese and livestock. Port Hedland has a semi-arid climate with a tropical Savanna climate influence. It is warm to hot all year round, with mean maximum temperatures of 36.4°C in January and 27.1°C in July. Port Hedland is a sunny region with the annual rainfall averages of 311.5 mm. The yearly DNI of Port Hedland is about 2,734 kWh/m^2/year.

Table 1
Annual DNI and the time period of the weather data for the locations of the study

Location	Latitude/ Longitude	Annual direct normal irradiance (kWh/m^2/y)	Weather data period
Port Hedland	–20.23°N/119.1°E	2,734	1982–1997
Abu Dhabi	24.43°N/54.65°E	2,294	1982–1999
Antofagasta	–23.43°N/–70.43°E	2,050	1984–1997
Kish	26.5325°N/53.9868°E	1,950	2007–2011

2.2. Abu Dhabi

Abu Dhabi (24.43°N, 54.65°E) is the capital and the second most populous city in the UAE. Abu Dhabi lies on a T-shaped island jutting into the Persian Gulf from the central western coast. The city proper had a population of 1.5 million in 2014. The city is the country's center of political and industrial activities, and a major cultural and commercial center, due to its position as the capital. Abu Dhabi is on the northeastern part of the Persian Gulf with the area of 972 km^2. This city has sunny blue skies throughout the year with extremely hot and humid weather conditions during the warm months having the maximum temperatures averaging above 38°C. The annual DNI for the Abu Dhabi is 2,294 kWh/m^2/year.

2.3. Kish Island

Kish Island (26.53°N, 53.96°E) with the area of 91 km^2 is a touristic place located on the north east of the Persian Gulf; about 17 km from the southern offshore of the mainland Iran. The island is positioned along the 1,359 km long Iranian coastline north of the Persian Gulf; at the first quarter from the Hormuz entrance to the Persian Gulf. Due to its free trade zone status, it is touted as a consumer's paradise with numerous malls, shopping centers, tourist attractions, and luxurious hotels. The yearly DNI of the study area is about 1,950 kWh/m^2/year. Although very hot and humid in summer, it has a pleasant weather from about November to March; with an annual average temperature of 27°C.

2.4. Antofagasta

Antofagasta is a port city and it is the capital of Antofagasta Province and Antofagasta Region. The city with the population of 345,420 is a major mining area of the Chile. The last decade has been a steady growth in the areas of construction, retail, hotel accommodations, population growth, and remarkable skyline development. There are many retail chains and supermarkets as well as various high-quality hotel chains, which promoted business tourism to attract capital and trading partners in mining and port activity. Antofagasta has a desert climate with abundant sunshine. The average annual temperature is 16.8°C with the highest and lowest temperatures of 30°C and 3°C, respectively. The solar radiation data of the Andrés Sabella Gálvez (23.43°S, 70.43°W) international airport located at 10 km north of the Antofagasta was used in the calculations of the present work. The yearly DNI of the described location is about 2,050 kWh/m^2/year. Fig. 1 shows the DNI solar radiation map of the study locations.

Figs. 2 and 3 show the monthly average daily global solar radiation for the locations of the study. As it is clear from Fig. 2, the monthly average daily global solar radiation of Port Hedland is higher than that of for the Antofagasta and it exceeds 1 kW/m^2 for 4 months of the year. According to Fig. 3, Abu Dhabi has higher monthly average daily global solar radiation level as compared with Kish Island.

The frequency of the DNI for four locations of the study is shown in Figs. 4(a) and (b) for the DNI values of less than and more than 400 W/m^2, respectively. As it is shown in Fig. 4(a), the frequency of the DNI with the values of less than 400 W/m^2 is equal to 64% and 73% for Port Hedland and Kish, respectively. Fig. 4(b) shows that Kish has highest frequency of the DNI for the values between 400 and 700 W/m^2. For the DNI values between 700 and 900 W/m^2, Abu Dhabi has the highest frequency among the other locations. Port Hedland with the frequency of 11% for the DNI values of more than and equal to 900 W/m^2 has the highest annual DNI among four locations of the study.

3. SRC/MED/LF plant

Fig. 5 shows the schematic diagrams of the proposed dual purpose SRC/MED/LF plant. As it is clear from Fig. 5, the SRC plant comprises of two low and high pressure turbines, two pumps, a feed water heater (FWH), two linear Fresnel (LF) solar fields and a condenser that is replaced by a low temperature MED unit. Two LF solar fields were considered in the present work; LF1 is considered to be used as the thermal source of the SRC during the day time and only for direct support of the SRC. The second solar field of LF2 was applied to store the thermal energy during day time and discharge that during the times between sunrise and sunset. The LF1 solar field was allowed to generate the output temperatures of equal to and less than 395°C and the shortage in the required thermal energy were considered to be supported by using an auxiliary natural gas boiler (NGB). The charging and discharging efficiency of 90% was considered in the calculations of the amount of available storable thermal energy in the present study.

3.1. Linear Fresnel solar field

LF uses several small flat optical mirrors that are positioned to reflect direct sunlight into a long receiver. LF collector comprises of the following components: (a) supporting structure and primary reflectors, (b) a receiver consisting of secondary reflectors and vacuum absorber tubes, (c) control systems for the primary reflector tracking and (d) the solar array output and hydraulic circuit to circulate the HTF through the receiver. Fig. 6 shows three main components of the LF reflector. When the sun rays fall on Fresnel mirror strip they get reflected from the mirror to the receiver.

The thermal output power of a LF is determined by considering the sun position at the respective hours during the year as well as the solar field optical and thermal efficiency models. The amount of heat available at the receiver of the LF is calculated using the following equations:

$$Q_{\text{in}} = \eta_{\text{opt}} . \eta_{\text{endloss}} . Q_{\text{absorbed}} \tag{1}$$

$$Q_{\text{absorbed}} = A_{\text{field}} . \text{DNI} \tag{2}$$

$$\eta_{\text{opt}} = \eta_{\text{opt\_0}} . \text{IAM}_t . \text{IAM}_L \tag{3}$$

$$\eta_{\text{endloss}} = 1 - \tan\theta_i . \frac{L_f}{L} \tag{4}$$

η_{opt}, $\eta_{\text{opt\_0}}$, η_{endloss} and A_{field} are the optical efficiency, the optical efficiency for normal incidence (0.65), end loss efficiency of the linear Fresnel receiver and the total collector

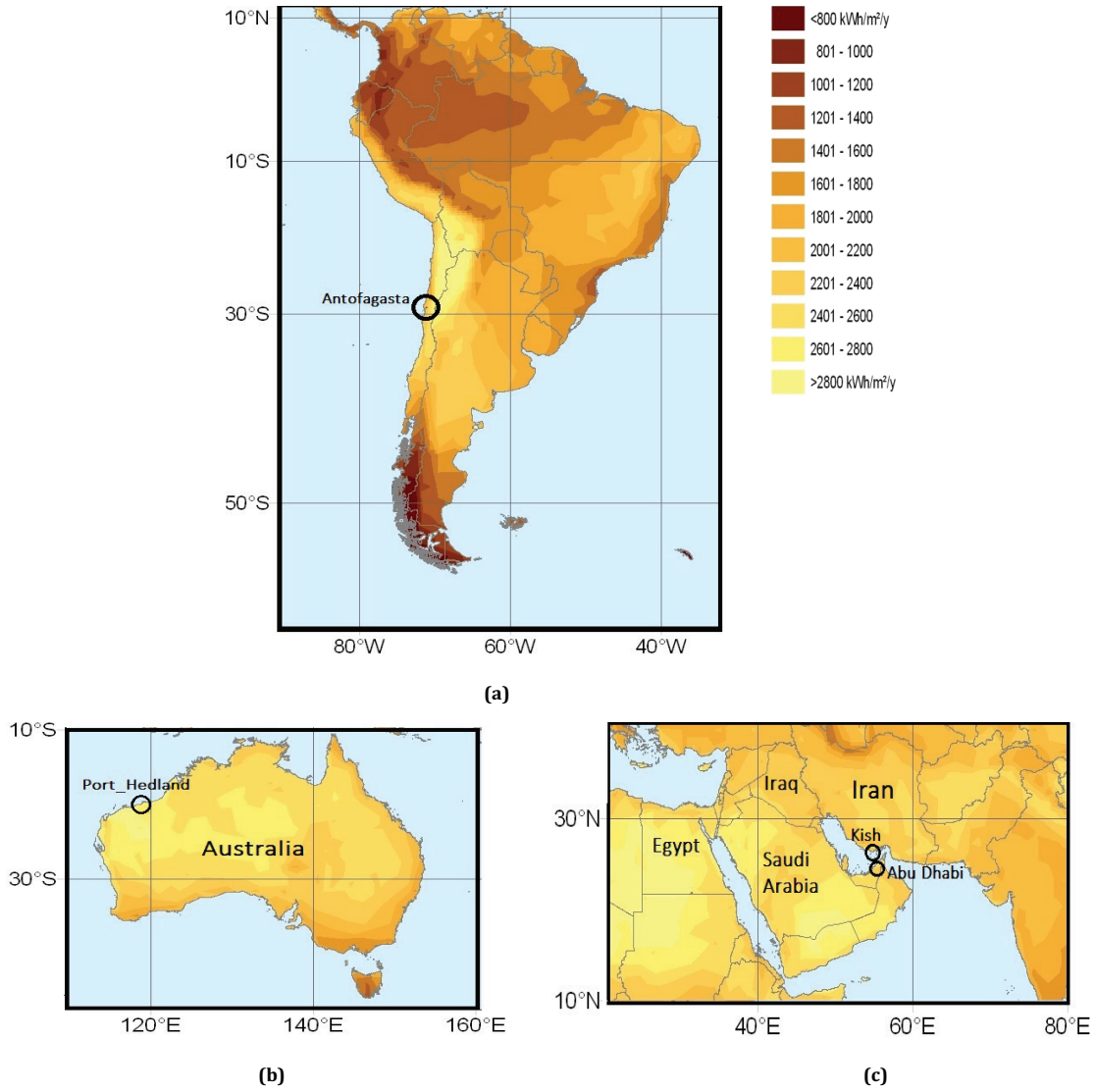

Fig. 1. Direct normal irradiance (DNI) for the locations of the study (July 1983–June 2005) [38]. (a) Antofagasta, Chile; (b) Port Hedland, Australia and (c) Kish Island and Abu Dhabi.

aperture area of the LF, respectively. θ_i, L_f and L are the incidence angle, the focal distance of primary mirrors from the tube absorber and the receiver length, respectively. IAM_t and IAM_L are the transversal and longitudinal incidence angle modifier (IAM), respectively. IAM_t and IAM_L consider the cosine effect, primary mirrors mutual blocking and shading, secondary reflector and support shading, optical properties variation and intercept factor modification [39]. Finally, the amount of the heat that is produced by the LF is calculated by considering the solar field piping heat losses as follows:

$$\dot{Q}_{LFR} = \dot{Q}_{in} - \dot{Q}_{hl_{HTF}} - \dot{Q}_{hl_{piping}} \quad (5)$$

where $\dot{Q}_{hl_{HTF}}$ is the heat loss from the LF receiver and $\dot{Q}_{hl_{piping}}$ is the heat loss from other pipes in the solar field per each square meter of the solar field collector aperture area (W/m^2) [40]. An average value of 10 W/m^2 was used in the calculations of the present study.

SAM software [41], provided by the National Renewable Energy Laboratory, was used for the calculations of the linear Fresnel field output thermal power. The solar radiation data, zenith and azimuth angles of the study locations were input in the SAM to calculate the hourly LF thermal output. The hourly optical efficiency of the solar field for two locations of the Kish and Port Hedland is shown in Figs. 7 and 8, respectively. As it is shown in these two figures, the maximum daily optical efficiency of the field varies between 0.4 and 0.65 for the both locations.

3.2. MED unit

The parallel feed configuration MED unit was considered in the present work in which the evaporating brine and heating steam flows have the same direction. The preheated feed sea water is divided into the set of parallel streams to feed into each evaporation effect. A train of flashing boxes, equal to $n-1$ number is used sometimes in the MED systems to use

the latent heat of the distillate water that is produced in the evaporator tubes of the previous effects. In order to enhance the feed water temperature, the preheaters are assigned to transfer part of the thermal energy of the output vapor of each effect to the feed sea water that is sprayed into that effect. The low temperature MED unit, which was previously investigated in reference [19] (MENA countries project), was considered to be used as the condenser of the SRC/LF plant. Fig. 9 shows the schematics of a parallel feed MED unit.

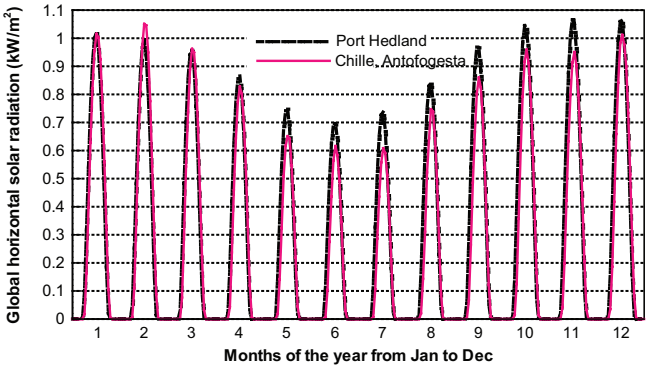

Fig. 2. Monthly average daily global solar radiation for Port Hedland and Antofagasta.

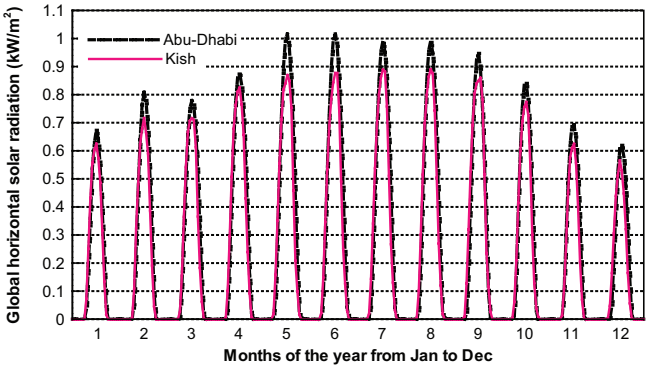

Fig. 3. Monthly average daily global solar radiation for Abu Dhabi and Kish.

As shown in Table 2, the target MED unit comprises of 14 effects with the GOR of 12, which means that the MED could produce 12 units of the fresh water per each unit of the heating steam that is flowed through its first effect. It was assumed that the desalination unit works at its optimum operation conditions. Also, in order to consider different water production rates (80,000, 120,000 and 160,000 m^3/d), the sizes of the MED unit was changed with assuming its constant GOR, constant top and minimum brine temperatures and also constant specific heat transfer area.

3.3. Solar Rankine cycle, thermodynamics modeling

The SRC operates at the pressure of 11,000 kPa and the inlet temperature of 395°C. The state point of "5" in Fig. 5 is the design temperature of 395°C that should be obtained by either solar field or natural gas (NG) auxiliary boiler. Also, the MED inlet temperature was considered as 72.5°C according to the specifications of the MED system that are shown in Table 2. A computer program was developed in MATLAB to model the thermodynamic procedures of the SRC and to determine the amount of the SRC mass flow rate, thermal efficiency, electricity generation rate, the amount of mass flow rate that should be introduced into the MED unit, percentage of the solar share as well as the required SM for different hours of thermal storage. Eqs. (6) and (7) were used to calculate the SRC HTF mass flow rate and the mass flow rate that should be flowed into the MED first effect, which is used as the condenser of the SRC.

$$\dot{m} = \frac{\dot{m}_c}{z \times (1-x)} \tag{6}$$

$$\dot{m}_c = \frac{\dot{m}_D}{\mathrm{GOR}} \tag{7}$$

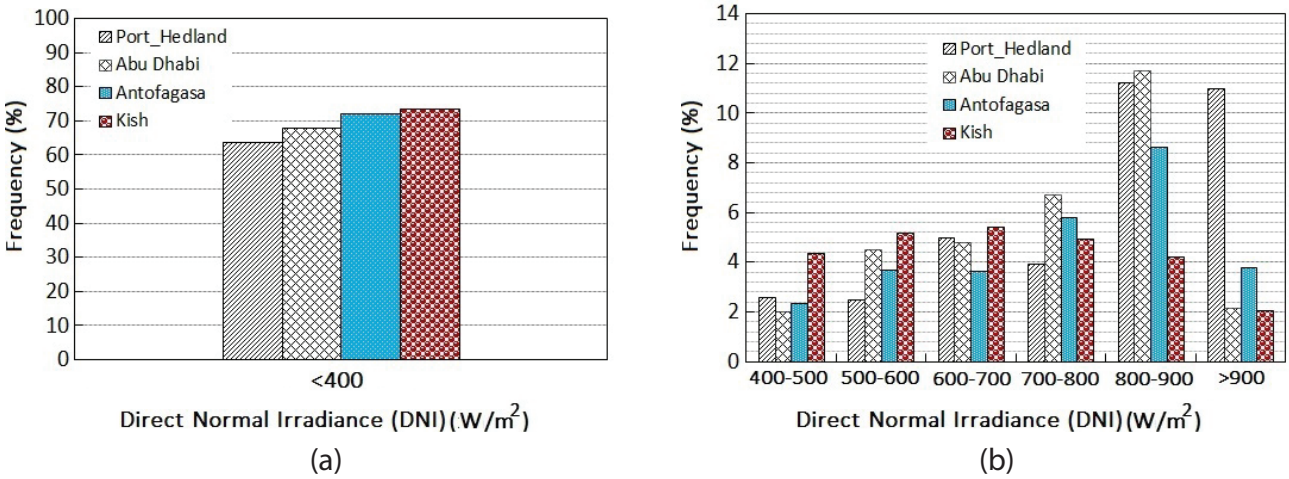

Fig. 4. Direct normal irradiance (DNI) frequency for the locations of the study. (a) Frequency of the DNI with the values less than 400 W/m². (b) Frequency of the DNI with the values more than 400 W/m².

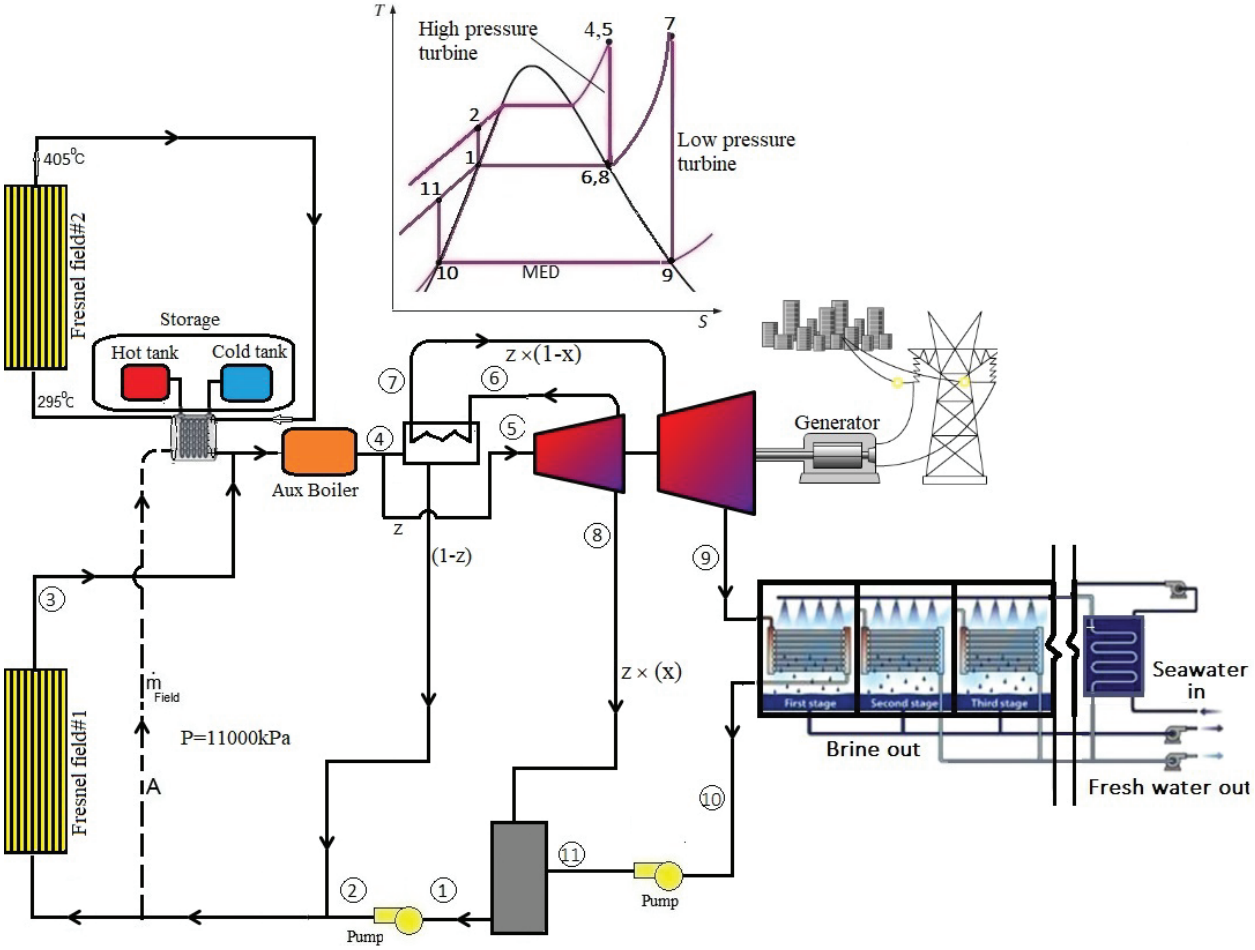

Fig. 5. Schematic of the SRC/MED/LF plant.

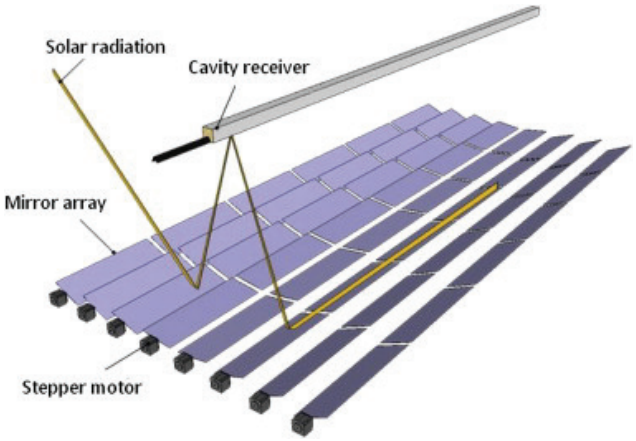

Fig. 6. Linear Fresnel (LF) reflector.

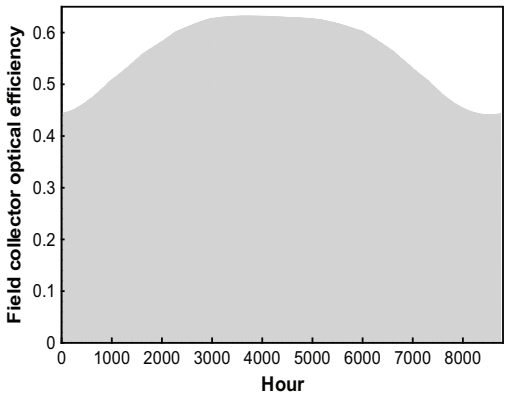

Fig. 7. Hourly optical efficiency of the field during the year, Kish Island.

where $\dot{m}$ and $\dot{m}_c$ are the solar field and condenser mass flow rates, respectively. GOR is the ratio of the distillate water mass flow rate to the heating steam mass flow rate ($\dot{m}_c$) that is flowing into the MED first effect. "z" is the fraction of solar field mass flow rate that is flowed into the high pressure steam turbine of the Rankine cycle (Fig. 5). x is the fraction of Rankine cycle mass flow rate that is extracted from the high pressure turbine outlet and its value was considered to be regulated according to the required pressure of the heating steam that is entered into the MED first effect. The lower water production capacities imply the lower solar field HTF mass flow rates and consequently the lower electricity production. The energy balance equations for SRC/MED/LF system are proposed in this section. The main assumptions used in the modeling of the present study are shown below:

- The MED unit works at its optimum operational conditions (Table 2).
- The SRC cycle operates at 395°C and 11,000 kPa.
- Both linear Fresnel fields operate at 11,000 kPa.
- Pumps and turbines efficiencies were considered as 85%.

Linear Fresnel solar field:

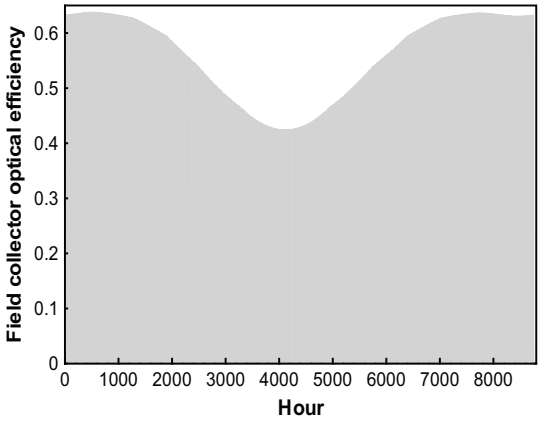

Fig. 8. Hourly optical efficiency of the field during the year, Port_Hedland.

$$\dot{Q}_{LFR} = \dot{m} \times (h_2 - h_3) \tag{8}$$

where $\dot{Q}_{LFR}$ is the amount of the heat that is produced by the LF.

Auxiliary boiler:

$$\dot{Q}_{NGB} = \dot{m} \times (h_3 - h_4) \tag{9}$$

where $\dot{Q}_{NGB}$ is the amount of heat that is supplied by NGB.

Regeneration heat exchanger:

$$\dot{m} \times (1-z) \times (h_4 - h_2) = \dot{m} \times z \times (1-x) \times (h_7 - h_6) \tag{10}$$

High pressure turbine:

$$\dot{m} \times z \times (h_5 - h_8) = \dot{W}_{HPT} \tag{11}$$

Low pressure turbine:

$$\dot{m} \times z \times (1-x) \times (h_7 - h_9) = \dot{W}_{LPT} \tag{12}$$

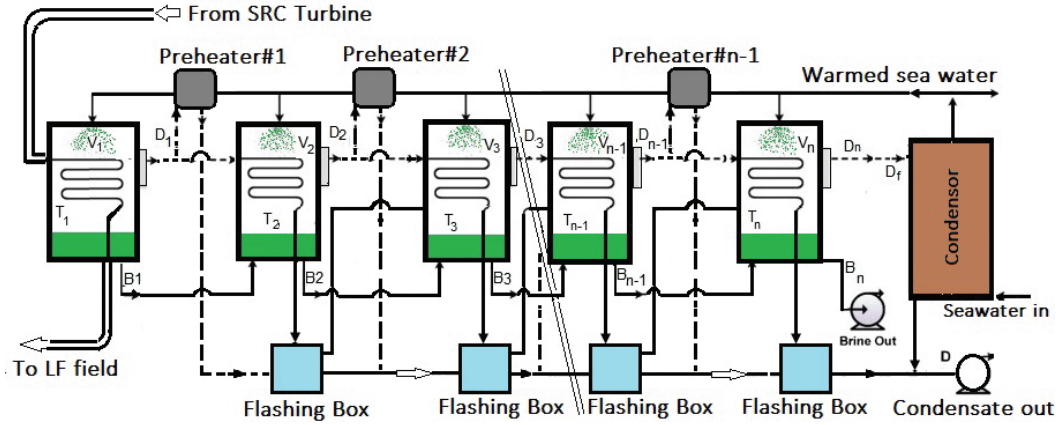

Fig. 9. Multi-effect desalination (MED) system parallel feed.

Table 2
Specifications of two commercial MED plants

Desalination plant	MENA project [19]	A	B	C
Operating and design conditions	MED			
Number of effects n	14	14	14	14
Top brine temperature T_1, °C	72.5	72.5	72.5	72.5
Cooling seawater temperature T_{cw}, °C	28	28	28	28
Heating steam flow rate D_s, kg/s	96.45	77.16	115.74	154.32
System performance				
Distillate production D_t, kg/s	1,157.40	925.92	1,388.88	1,851.85
Distillate production D_t, m3/d	100,000	80,000	120,000	160,000
Gain output ratio GOR	12	12	12	12
Specific heat consumption Q, kJ/kg	194.36	194.36	194.36	194.36

$\dot{W}_{HPT}$ and $\dot{W}_{LPT}$ are high pressure and low pressure turbine output electricity work, respectively.

MED unit:

$$\dot{Q}_{S\_MED} = \dot{m} \times z \times (1-x) \times (h_9 - h_{10}) \quad (13)$$

In the above equation, $\dot{Q}_{S\_MED}$ is the MED heating steam thermal energy.

Pump#1:

$$\dot{m} \times z \times (1-x) \times (h_{10} - h_{11}) = \dot{W}_{P1} \quad (14)$$

Mixing chamber:

$$\dot{m} \times z \times (1-x) \times (h_{11}) + \dot{m} \times z \times (x) \times (h_8) = \dot{m} \times z \times h_1 \quad (15)$$

Pump#2:

$$\dot{m} \times z \times (h_1 - h_2) = \dot{W}_{P2} \quad (16)$$

W_P is the pump required work.

TES system:

LF2 was considered in order to charge the TES system during the daytime. The charging and discharging processes of the storable thermal energy was calculated using the following equations:

$$\dot{Q}_{Ch} = \eta_{Ch} \times \dot{Q}_{LF2} = \eta_{Ch} \times \dot{m}_{HTF} \times \left(h_{hot} - h_{cold}\right) \quad (17)$$

$$\dot{Q}_{TES} = \dot{Q}_{Disch} = \eta_{Disch} \times \dot{Q}_{Ch} = \eta_{Ch} \times \eta_{Disch} \times \dot{m}_{HTF} \times \left(h_{hot} - h_{cold}\right) \quad (18)$$

where h_{hot} and h_{cold} are the thermal energies of the HTF in the inlet and outlet of the solar field, respectively, and $\dot{m}_{HTF}$ is the HTF mass flow rate. $\dot{Q}_{LF2}$ is the solar field (LF2) thermal energy, $\dot{Q}_{Ch}$ is the thermal energy that is stored in the hot storage tank and Q_{Disch} is the discharged thermal energy or thermal energy that could be supplied by TES system. η_{Ch} and η_{Disch} are the charging and discharging efficiencies, respectively, which were considered as 90% in the present study.

Natural Gas Boiler (NGB):

A heat exchanger with the efficiency (η_{Hex}) of 90% was considered in order to transfer the thermal energy of the fossil fuel into the HTF. The thermal energy of the NGB, $\dot{Q}_{NGB}$, was calculated using the following equation:

$$\dot{Q}_{NGB} = \frac{\dot{Q}_{shortage}}{\eta_{Hex}} = \frac{\dot{m} \times \left(h_{T=395^\circ C} - h_3\right)}{\eta_{Hex}} \left(h_3 < h_{T=395^\circ C}\right) \quad (19)$$

where $\dot{Q}_{shortage}$ is the shortage in the HTF thermal energy and "$\dot{m}$" is the mass flow rate of the SRC plant.

The solar share definition, which is defined as the portion of solar contribution in supporting the required thermal energy of the SRC ($\dot{Q}_{need}$), was used in the present study.

$$\text{S-SH} = \frac{\sum_{t=1}^{t=8760} ((\dot{Q}_{LFR}(t) + \dot{Q}_{TES}(t))}{8760 \times \dot{Q}_{need}} \quad (20)$$

SM is a multiple of the aperture area required to operate the power cycle at its design capacity and it is calculated using the following equation:

$$\text{SM} = \eta_{th\_SRC} \cdot \frac{\text{Solar field Thermal output(MWt)}}{\text{SRC design output power(MWe)}} \quad (21)$$

where the solar field thermal output in the above formulation is calculated at the design point direct normal radiation which was considered as 950 W/m^2 in the present study. The flowchart diagram of the computer program that was used in thermodynamic modeling of the SRC/MED/LF plant is shown in Fig. 10. $\dot{Q}_{Def}$ in Fig. 10 refers to the hourly solar thermal power that is defocused to prevent the overheating of the LF output steam. The output results of the first computer program were used as the input parameters of the second economic sub-program.

4. Economic parameters

The capital direct (DC) and indirect (IC) costs as well as operation and maintenance costs of the SRC/MED/LF system were considered in the economical analysis. The capital costs of the MED and solar field are classified as DC and IC. The DC and IC of the project could be calculated in terms of the annualized capital costs using the capital recovery factor during the life time of the project (N) and considering the real interest rate of i as follows:

$$C_{CAPEX} = C \times \text{CRF}(i, N) \quad (22)$$

$$\text{CRF}\left(i, N\right) = \frac{i.(1+i)^N}{(1+i)^N - 1} \quad (23)$$

The operation and maintenance costs comprise of the insurance cost (C_{Ins}), labor cost (C_L), spare parts replacement cost (C_{SP}), fuel cost (C_f) and electricity cost (C_{el}). The operation and maintenance costs of the desalination units were determined as the percentages of their direct costs and also based on their electrical end thermal energy costs. Two economic definitions of the LCOE and the LCOW were used in the economic calculations. The following formulation of LCOE and LCOW was used to calculate the electricity and water unit of costs based on the capital annualized direct (C_{CAPEX}(D)) and indirect costs (C_{CAPEX}(ID)) [42]:

$$\text{LCOE} = \frac{\left[C_{CAPEX}\left(D\right) + C_{CAPEX}\left(\text{ID}\right) + C_{Ins} + C_L + C_{SP} + C_{el}\right]_{LF_{solar_{field}}}}{\text{TAEG}} + \frac{\left[C_{CAPEX}\left(D\right)\right]_{Boiler\_Backup} + C_f}{\text{TAEG}} \left(\frac{\$}{\text{kWh}}\right) \quad (24)$$

$$\mathrm{LCOW}=\frac{\left[C_{\mathrm{CAPEX}}(D)+C_{\mathrm{CAPEX}}(\mathrm{ID})+C_{\mathrm{Ins}}+C_{L}+C_{\mathrm{SP}}+C_{\mathrm{el}}\right]_{\mathrm{MED}}}{\mathrm{TAWP}}+\frac{\left[C_{\mathrm{CAPEX}}(D)-\mathrm{PB}+C_{\mathrm{CAPEX}}(\mathrm{ID})+C_{\mathrm{Ins}}+C_{L}+C_{\mathrm{SP}}+C_{\mathrm{el}}\right]_{\mathrm{LF}_{\mathrm{solar_{field}}}}}{\mathrm{TAWP}}+\frac{\left[C_{\mathrm{CAPEX}}(D)\right]_{\mathrm{Boiler\_Backup}}+C_{f}}{\mathrm{TAWP}}\left(\frac{\$}{\mathrm{m}^{3}}\right) \quad (25)$$

where TAEG and TAWP are the total annual electricity generation (kWh/year) and water production (m^3/year), respectively. In the calculations of the present study, the real interest rate (i) and project life time (N) were considered as 6% and 25 years, respectively. Table 3 shows the capital and operational and maintenance costs of the MED desalination unit and also the investment costs of a LF solar field (with a power block).

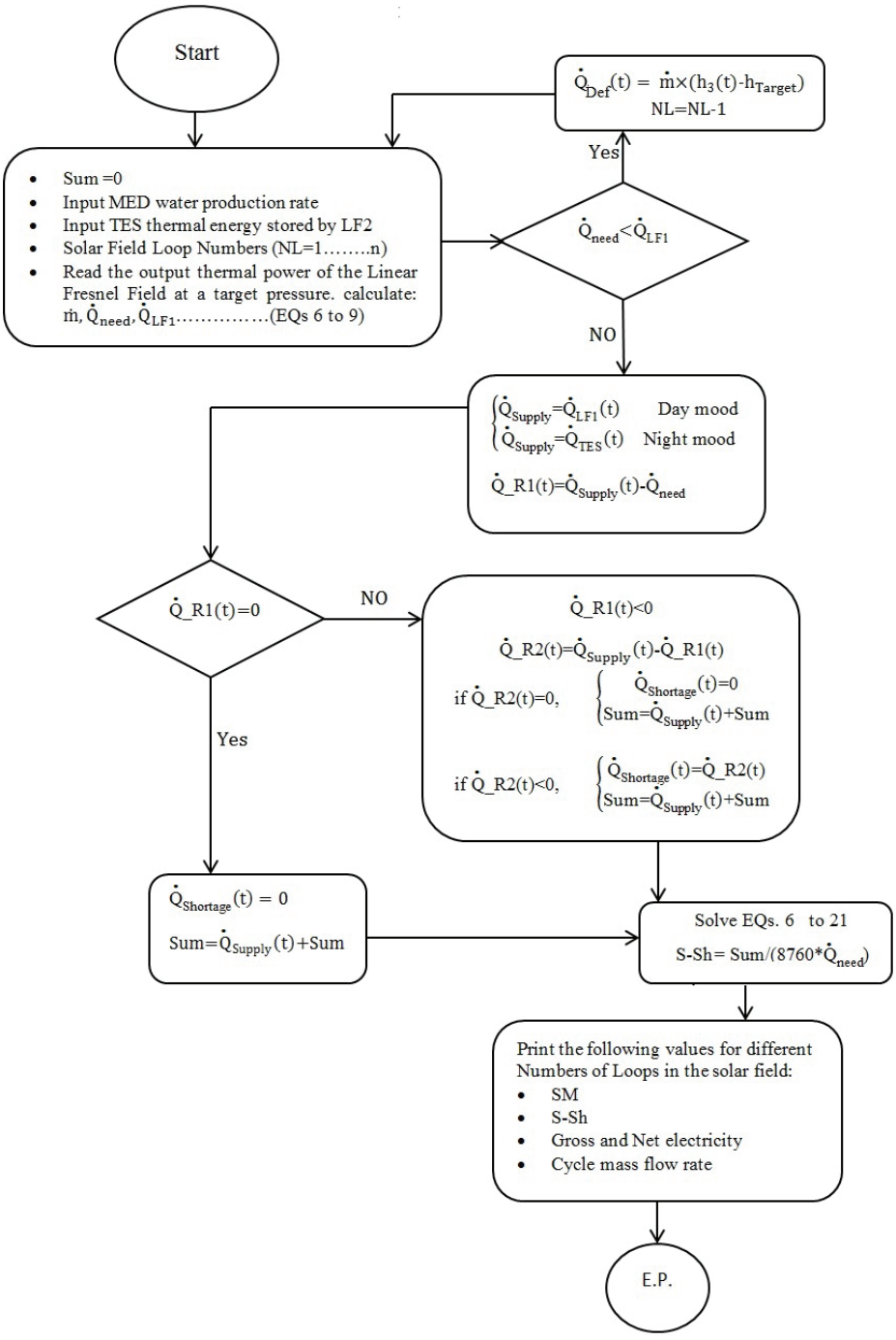

Fig. 10. Flowchart diagram of the thermodynamic modeling of the SRC/MED/LF plant.

Table 3
Different cost parameters of the linear Fresnel solar field, MED desalination unit [19,41,42]

MED (100,000 m^3/d)	
Direct costs (DC)	
Main investment ($/$m^3$/d)	1,700
Post-treatment plant ($/$m^3$)	120
Open sea water intakes ($/$m^3$)	313
Drinking water storage and pumping ($/$m^3$)	100
Water storage tank ($/$m^3$/h)	100
Indirect costs (IC)	
Freight and insurance rate during construction	5.00% DC
Owner's cost rate	10.00% of direct material and labor cost
Contingency rate	10.00% of DC
Construction overhead (interest during construction)	12.24% of DC
Operation costs (OC)	
Electricity costs ($/$m^3$)	0.315 (Assuming: 1.5 kWh/m^3)
Spare parts replacement	1.5% of total DC
Chemical cost of product water ($/$m^3$)	0.025
Insurance	5.00% of total DC
Natural gas auxiliary boiler costs ($/$m^3$)	0.02
Labor cost of product water ($/$m^3$)	0.025
Linear Fresnel solar field and power block	
Direct costs (DC)	
Site improvement ($/$m^2$)	20
Solar field ($/$m^2$)	180
HTF system ($/$m^2$)	35
Electricity costs ($/kWh)	0.21
Thermal storage system ($/kWht)	70
Contingency rate	10.00% total DC
Power block (PB) ($/kWh)	940
Indirect costs (ID)	
Design and construction	15% of total DC
Land cost ($/$m^2$)	10
Insurance	1% of total DC

5. Results and discussions

A computer program was developed in MATLAB and the hourly solar thermal power of the LF solar field that is determined by SAM was applied in the MATLAB program. The LF solar field with 13 numbers of modules in each loop, the total aperture area of 6,676.8 m^2 for each loop and considering evacuated tube model for the receivers was applied in the calculations of the present research.

5.1. SRC operational conditions

The calculation procedures were done to determine the temperature, pressure and thermal energy of each point that are formerly shown in Fig. 5. Based on the SRC operational pressure and temperature (11,000 kPa, 395°C) and considering the MED required heating dry steam of 72.5°C, the thermodynamic state of each point for the SRC/MED/LF plant is obtained as it is tabulated in Table 4.

Table 4
Thermodynamic properties of the state points of the configuration '*A*' that are shown in Fig. 5

Point	Pressure (kPa)	Temperature (°C)	*h* (kJ/kg)
1	1,050	182	772.3
2	11,000	182	773.5
3	11,000	Variable	Variable
4 and 5	11,000	395	3,057
6	1,050	182	2,646
7	1,050	395	3,252
8	1,050	182	2,646
9	34.72	72.5	2,630
10	34.72	72.5	304
11	1,050	72.5	304

The effect of increasing of the MED water production capacity on the SRC HTF mass flow rate, MED required heating mass flow rate, gross and net electricity generation rates were also considered to determine the SM, solar share, LCOE and LCOW of the SRC/MED/LF plant with different water production and electricity generation rates. Table 5 shows the HTF and MED heating mass flow rates for different water production capacities.

5.2. Field output temperature control strategy

The output temperature of the solar field was considered to be regulated by using of defocusing the solar field mirrors. Fig. 11 shows the defocused fraction of the solar field for two regions of Kish Island and Port Hedland when 80 numbers of loops are used in the LF solar field. As it is shown in Fig. 11, in order to prevent the overheating of the solar field during the warm months and to keep the solar field output temperature at 395°C, part of the mirrors should be defocused. A comparison between Figs. 11(a) and (b) shows that Port Hedland with higher DNI level has higher defocused fractions during its warm months as compared with the Kish Island.

5.3. SRC/MED/LF system without thermal storage

At the first part of the study, the SRC/MED/LF was considered without TES system. Fig. 12 shows the effect of increasing of the solar field number of loops on the percentage of the solar share for four locations of the study. As it is evident from Fig. 12, the increasing of the number of the loops for more than 110 numbers has no considerable effect on the percentage of the solar share. Fig. 12 also shows that the application of the SRC/MED/LF plant in a location such as the Port Hedland with annual DNI of 2,734 kWh/m^2 has highest percentage of solar share as compared with the cases that the SRC/MED/LF plant located in the other locations. For 110 numbers of the loops in the LF solar field, the percentage of the solar share for SRC/MED/LF plant located in Port Hedland, Abu Dhabi, Antofagasta and Kish Island is obtained as 28%, 24%, 21.5% and 19.5%, respectively. Fig. 13 shows the variation of the plant LCOE vs. the solar field numbers of

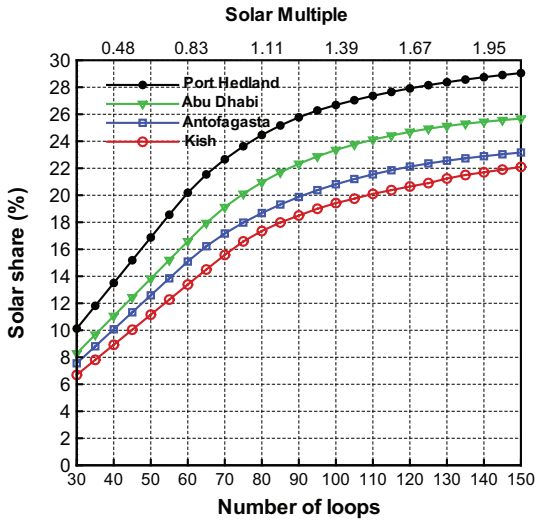

Fig. 12. Solar share of the SRC/MED/LF plant without TES.

Table 5
SRC HTF and MED mass flow rates of the configuration '*A*' at different water production capacities

Solar field HTF mass flow rate (kg/s)	MED heating mass flow rate (kg/s)	Water production rates (m^3/d)	Gross electricity (MW)	Net electricity (MW)
96.45	77.16	80,000	84.96	71.46
144.67	115.74	120,000	130.01	110.05
192.20	154.32	160,000	174.46	146.67

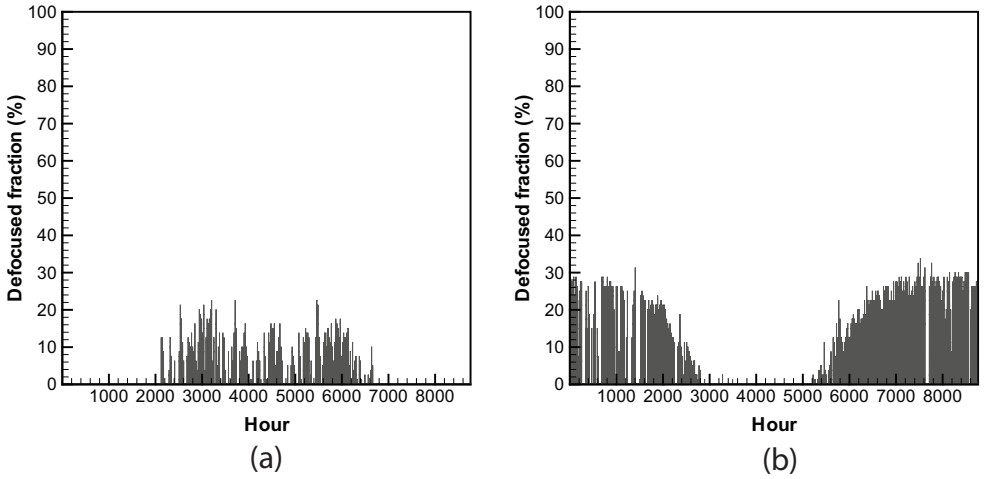

Fig. 11. Solar field defocused fraction, without thermal storage $\dot{m} = 340000\text{kg/h}$, loop number = 80, SM = 1.11, field pressure = 11,000 kPa, T_{in} = 182°C, net electricity rate = 85 MW. (a) Kish, solar share = 17.34%, (b) Port Hedland, solar share = 25%.

loops. As it is shown in this figure, the increasing of the number of loops to 80 numbers would result in decreasing of the plant LCOE and further increase in the solar field number of loops increases the LCOE of the plant.

The percentage of the solar share for 6 h of thermal storage is shown in Fig. 14. The SRC/MED/LF plant with 170 numbers of loops and 6 h of thermal storage has the solar share of 44%, 38%, 34% and 31.78% for Port Hedland, Abu Dhabi, Antofagasta and Kish Island, respectively. The minimum LCOE of the plant with 6 h of thermal storage would be obtained for the LF solar field with 170 numbers of loops as it is shown in Fig. 15. The results of Figs. 12–15 show that the integration of 6 h of thermal storage results in nearly 82% increase in the percentage of the solar share and 20% increase in the LCOE of the plant.

The effect of increasing of the solar field number of loops on the LCOW of the SRC/MED/LF plant is shown in Fig. 16 for 6 h of thermal storage. According to this figure, the LCOW of the system with the minimum LCOE (170 numbers of loops) is obtained as 1.47, 1.54, 1.61 and 1.68 $/m^3 for Port Hedland, Abu Dhabi, Antofagasta and Kish Island, respectively. The effect of increasing of the thermal storage hours on the solar share, solar multiple, LCOE and LCOW of the SRC/MED/LF plant with minimum LCOE are shown in Figs. 17 and 18. As it is shown in Figs. 17 and 18, the percentage of the solar share and SM of the system with the minimum LCOE would be increased by about 19.60%, 39.83% and 55.51% by increasing of the thermal storage hours from 6 to 9 h, 12 h and 15 h increases, respectively.

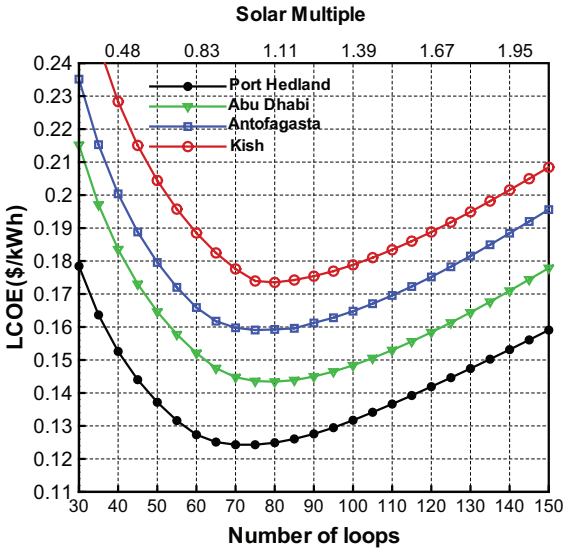

Fig. 13. LCOE of the SRC/MED/LF plant without TES.

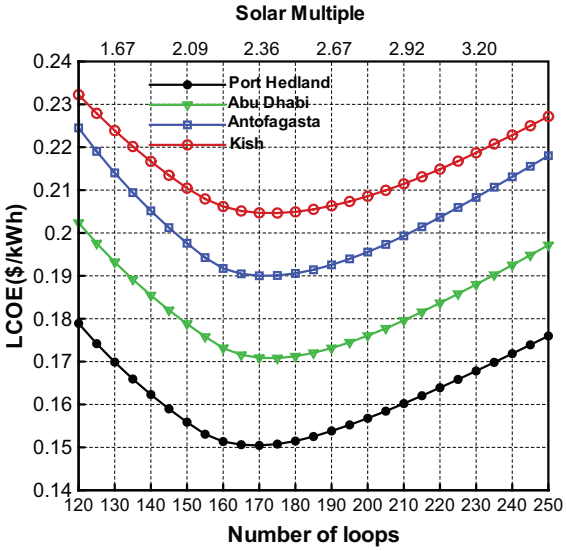

Fig. 15. LCOE of the SRC/MED/LF plant with 6 h of thermal storage.

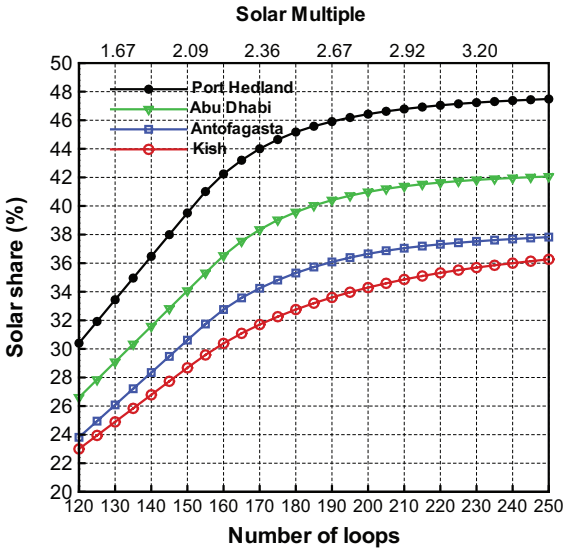

Fig. 14. Solar share of the SRC/MED/LF plant with 6 h of thermal storage.

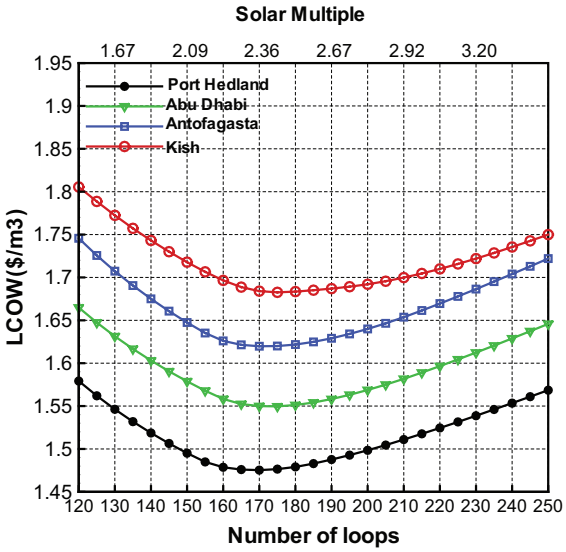

Fig. 16. LCOW of the SRC/MED/LF plant with 6 h of thermal storage.

Fig. 19 shows that, for the SRC/MED/LF plant that is considered to be located in the Port Hedland, the minimum LCOE of the plant would be increased by about 2.14%, 3.61% and 4.45% by increasing the thermal storage hours from 6 to 9 h, 12 h and 15 h, respectively. However, for the Kish Island with the lowest annual DNI level among the locations of the study, the percentage increase in the minimum LCOE of the system would be obtained as 3.17%, 5.37% and 7.70% by increasing the thermal storage hours from 6 to 9 h, 12 h and 15 h, respectively. Fig. 20 shows that the increasing of the thermal storage hours from 6 to 9 h, 12 h and 15 h would result 0.79%, 1.34% and 1.65% increase in the LCOW of the system, respectively, for the plant located in Port Hedland. For the Kish Island, the LCOW of the plant would be increased by about 3.44% with increasing the thermal storage hours from 6 to 15 h.

5.4. Validation of the results

As it is mentioned in the introduction section, the investigation of the LF solar field to produce the electricity and water has been rarely reported in the previous research works. Cocco and Cau [9] performed a comparison between the PTC and LF solar fields to produce the electricity through a SORC plant when it is located in Cagliari with total annual DNI of 1,720 kWh/m^2/year and considering a design point DNI of 800 W/m^2. As it is clear from Fig. 21, the authors of that study had shown that the required SM for a SORC/LF plant is obtained as approximately equal to 1.2, 1.9, 2.7 and 3.2 for cases without thermal storage, 4, 8 and 12 h of thermal storage, respectively. The comparison between Figs. 18 and 21 shows that the results of the present paper for the SM are in good agreement with the results reported in the study by

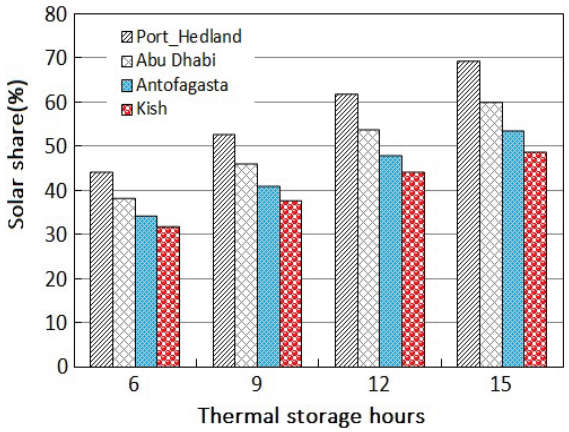

Fig. 17. Effect of thermal storage hours on the percentage of solar share for the systems with minimum LCOE.

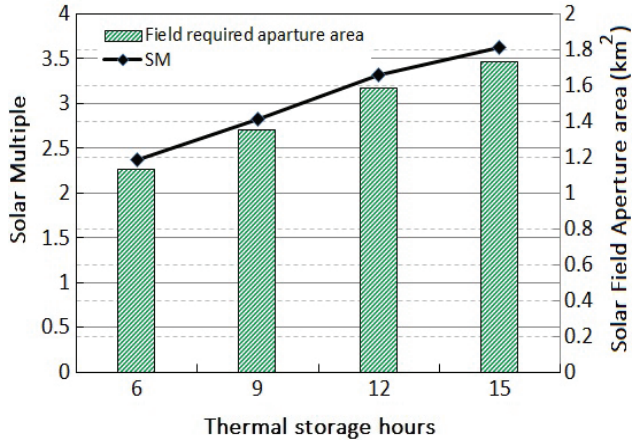

Fig. 18. Required SM to have the minimum LCOE for different thermal storage hours.

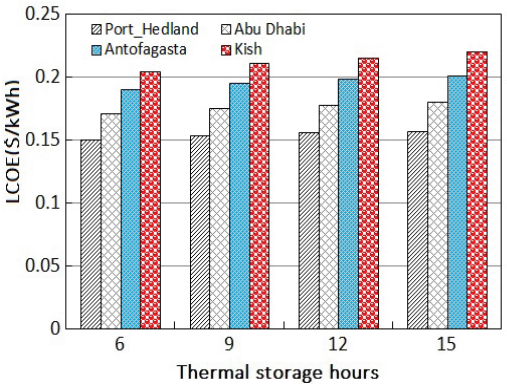

Fig. 19. Effect of thermal storage hours on the minimum LCOE of the plant.

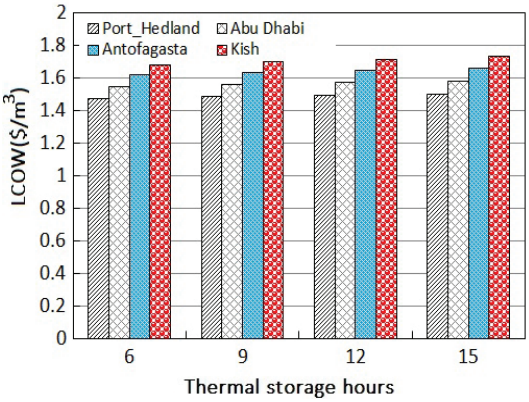

Fig. 20. Effect of thermal storage hours on the LCOW of the plant with minimum LCOE.

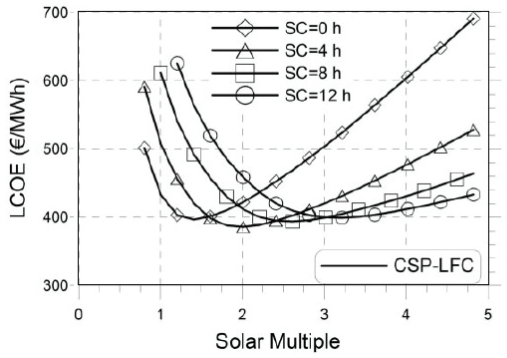

Fig. 21. SM values for different thermal storage hours [9].

Cocco and Cau [9]. However, in that study the gross electricity generation rate of 1 MW was considered for the SORC plant, which is considerably low as compared with the SRC plant that is proposed in the present paper; with the electricity generation rate of 85 MW. Therefore, the LCOE of the plant that is considered in the above study is considerably high as compared with the LCOEs that are obtained for the large-scale SRC plant proposed in the present paper.

The other reference that could be used to validate the results of the present paper is the research work which was performed by Fichtner and DLR [19] to investigate the dual purpose SRC/PTC/MED plant electricity and water costs. In that study, the SRC/PTC/MED plant with gross electricity generation rate of 107 MW and water production rate of 100,000 m^3/d was considered for the regions with different annual DNI levels of 2,000, 2,400 and 2,800 kWh/m^2/year. The results of that research work ([19]; pp. 157–160) have shown that for the regions with annual DNI levels of 2,000 and 2,400 kWh/m^2/year, the percentage of solar share would be obtained as 38.8% and 45.7%, respectively, for 7.5 h of thermal storage. According to Fig. 17, the percentage of the solar share for the SRC/MED/LF for 7.5 h of thermal storage could be estimated as approximately 35% and 42% for the total annual DNI levels of 2,000 and 2,300 kWh/m^2/year, respectively. Also, the results of Fichtner and DLR [19] demonstrated that depending on the total annual DNI level and the salinity of the seawater (between 39,000 and 46,000 ppm), the LCOE of the plant would be obtained as a value between 0.21 and 0.24 $/kWh for 7.5 h of thermal storage.

5.5. Sensitivity analysis

In order to determine that to what extend the LCOE and LCOW of the plant are sensible to the main cost parameters such as solar field (SF), TES and fuel prices, a sensitivity analysis was performed in this part of the study. In this regard, the LCOE and LCOW of the SRC/MED/LF plant were calculated when the solar field cost, TES cost and fuel cost are varied between the values less than and more than the first cost assumptions of Table 5. For instance, the solar field cost was considered to be varied from 80 to 288 $/$m^2$, which is, respectively, corresponding to 0.44-fold and 1.6-fold of the first cost assumption for the solar field (180 $/$m^2$). The sensitivity spider graphs for LCOE and LCOW of two locations of the study with highest and lowest annual DNI are shown in Figs. 22 and 23 for two thermal storage hours of 6 and 12 h, respectively. As it is shown in these figures, the LCOE and LCOW of the plant are more sensible to the solar field cost and the TES cost is the second important cost parameter that affects the LCOE and LCOW of the plant. The variation in the fuel price has a minimal effect on the system costs as compared with solar field and TES costs. As it is clear from Figs. 22 and 23, the slope of the SF and TES cost lines for the Kish Island is slightly more than that of for the Port Hedland, which has the highest annual DNI level. It could be concluded that the sensitivity of the LCOE and LCOW of a SRC/MED/LF plant to the SF costs is higher for the locations with lower annual DNI level. A comparison between Figs. 22 and 23 shows that the increasing of the thermal storage hours increases the sensitivity of LCOE and LCOW of the plant to the TES costs; this is why the slope of the TES cost line for 12 h of thermal storage in Fig. 23 is steeper than that of for 6 h of thermal storage (Fig. 21). The sensitivity of the LCOW of the plant to the SF cost, TES cost and fuel cost parameters is shown in Figs. 24 and 25 for Kish Island and Port Hedland, respectively, when 6 h of thermal storage are considered in the calculations. For both locations, the sensitivity of the plant LCOW to the TES cost would be increased by increasing the thermal storage capacity. Also, a comparison between

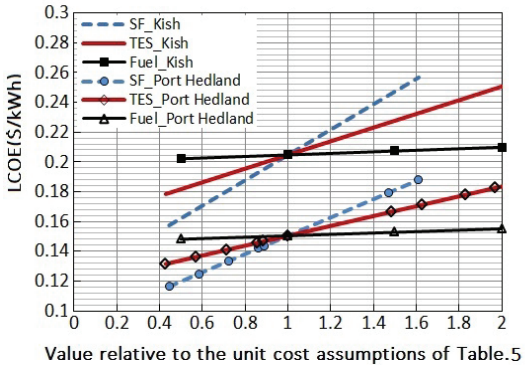

Fig. 22. Sensitivity of the LCOE to the cost parameters for 6 h of thermal storage.

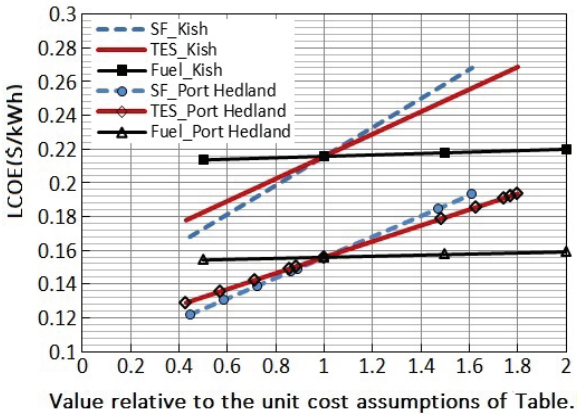

Fig. 23. Sensitivity of the LCOE to the cost parameters for 12 h of thermal storage.

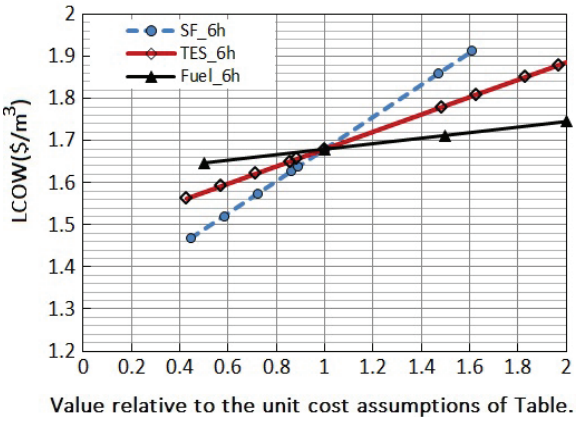

Fig. 24. Sensitivity of the LCOW to the cost parameters for 6 h of thermal storage, Kish Island.

Figs. 24 and 25 shows that the slope of the SF cost and TES cost lines for the Kish Island is higher than that of for the Port Hedland.

5.6. Effect of system scale on the LCOE and LCOW

The effect of increasing of the plant scale on the LCOE and LCOW was considered in this section. It has been proven that the larger scales of a plant could decrease the LCOE and LCOW of the system to the lower values [28,42]. The SRC/MED/LF plant was considered to produce larger water production rates of 120,000 and 160,000 m^3/d with net electricity generation rates of 110 and 146 MW, respectively. The following formulation was used in the calculations to determine the solar field, TES and MED capital costs for the systems delivering the larger capacities:

$$\frac{\text{Capital cost}_{\text{L\_scale}}}{\text{Capital cost}_{\text{S\_scale}}} = \left(\frac{\text{Capacity}_{\text{L\_scale}}}{\text{Capacity}_{\text{S\_scale}}}\right)^{n} \quad (26)$$

The exponent n in the above equation was considered as 0.65 and 0.82 for solar field (and TES system) and MED unit, respectively [42]. Fig. 26 shows the effect of increasing of the plant scales on its LCOE and LCOW when 6 and 12 h of thermal storage were considered in the calculations. As it is shown from Fig. 26, the increasing of the plant scales results in increasing of the water production and electricity generation rates, which that consequently decreases the LCOE and LCOW of the plant. According to Fig. 26, for both thermal storage hours the increasing of the water production rate from 80,000 to 120,000 m^3/d and 160,000 m^3/d would result in decreasing of the plant LCOE by about 9.22% and 14.16%, respectively. Also, the LCOW of the plant is decreased by about 11.10% and 18.50% by increasing of the plant water production rate from 80,000 to 120,000 m^3/d and 160,000 m^3/d, respectively. The similar results were obtained for the other locations of the study.

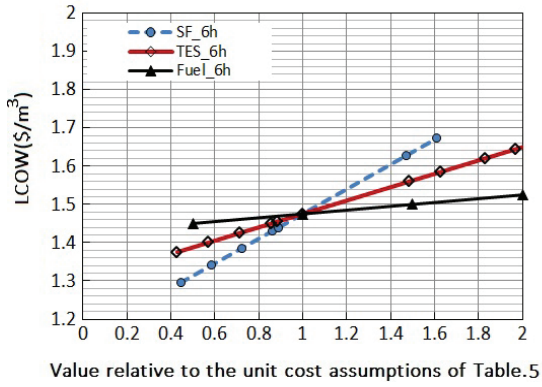

Fig. 25. Sensitivity of the LCOW to the cost parameters for 6 h of thermal storage, Port Hedland.

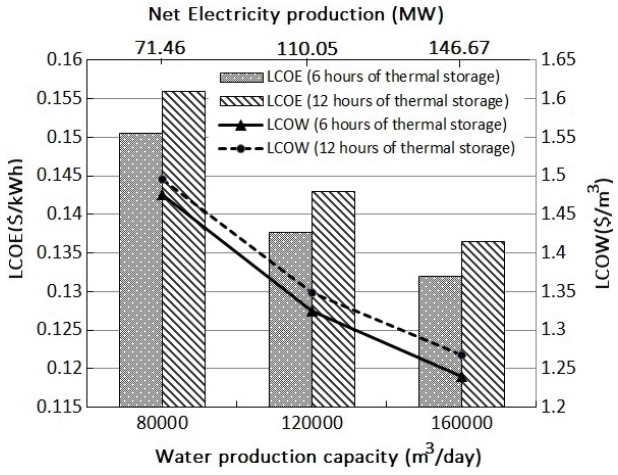

Fig. 26. Effect of increasing the system scale on the LCOE and LCOW for Port Hedland.

6. Conclusion

A dual purpose linear Fresnel SRC integrated with a MED was considered to generate the electricity and distillate water when it is located in four regions with different annual solar DNI levels. Part of the required thermal power of the cycle is supplied by solar field and a NGB was considered to be used as an auxiliary thermal source during the non-availability of solar thermal power. A typical MED unit with 14 effects and a daily water production rate of 80,000 m^3/d was considered to be used as the condenser of the described cycle. For all locations of the study, the water production cost (LCOW) and electricity generation cost (LCOE) of the described plant were determined for different thermal storage hours. The following results were obtained from this study:

- The application of the SRC/MED/LF plant in a region such as Port Hedland with annual DNI of 2,734 kWh/m^2/year results in 28% of contribution of the solar energy in required thermal power of the described plant when no thermal storage system is considered in the calculations. Also, the percentages of solar share for the SRC/MED/LF plant without thermal storage and located in Kish, Antofagasta and Abu Dhabi were obtained as 19.5%, 21.5% and 24.2%, respectively.
- For 6, 9, 12 and 15 h of thermal storage, the percentage of solar share was obtained as 44.00%, 52.77%, 61.78% and 69.07%, respectively, if the plant is considered to be located in Port Hedland. For Kish Island having the annual DNI of 1,950 kWh/m^2/year, 31.72%, 37.73%, 44.00% and 48.62% of solar share is obtained for 6, 9, 12 and 15 h of thermal storage, respectively. Generally, for all locations of the study 19.60%, 39.83% and 55.51% increase in the percentage of solar share is obtained by increasing of the thermal storage hours from 6 to 9 h, 12 h and 15 h, respectively.
- The SM for the SRC/MED/LF plant with 6, 9, 12 and 15 h of thermal storage was determined as 2.36, 2.82, 3.31 and 3.62, respectively.
- The LCOE of the plant with 6 h of thermal storage was obtained as 0.1504, 0.17.08, 0.1900 and 0.2046 $/kWh for Port Hedland, Abu Dhabi, Antofagasta and Kish, respectively. The increasing of the thermal storage hours from 6 to 15 h results in increasing of the LCOE by about 4.49% and 7.70% for the plant that is considered to be located in Port Hedland and Kish, respectively.

- The sensitivity analysis shown that both LCOW and LCOE are most sensitive to solar field costs. TES and fuel price are the second and third most sensitive parameters, respectively.
- The increasing of the plant scale, which results in increasing of the water production capacity from 80,000 to 160,000 m^3/d of fresh water, decreases the LCOE and LCOW of the plant by about 14.16% and 18.5%, respectively.

Symbols

A_{field}	—	Solar field aperture area, m^2
C_{CAPEX}(D)	—	Capital annualized direct costs, $
C_{CAPEX}(ID)	—	Capital annualized indirect costs, $
C_{el}	—	Electricity cost, $
C_f	—	Fuel cost, $
C_{Ins}	—	Insurance cost, $
C_L	—	Labor cost, $
CRF	—	Capital recovery factor
C_{SP}	—	Spare parts replacement cost, $
CSP	—	Concentrating solar power plant
DNI	—	Direct normal irradiation, W/m^2
GOR	—	Gain output ratio
h_{in}	—	Enthalpy of the heat transfer fluid at the inlet, kJ/kg
h_{out}	—	Enthalpy of the heat transfer fluid at the outlet, kJ/kg
HTF	—	Heat transfer fluid
IAM_t	—	Transversal incident angle modifier
IAM_L	—	Longitudinal incident angle modifier
ISCC	—	Integrated solar combined cycle
i	—	Interest rate, %
L	—	Receiver length, m
LCOE	—	Levelized cost of electricity, $/kWh
LCOW	—	Levelized cost of water, $/$m^3$
L_f	—	Focal distance, m
LF	—	Linear Fresnel solar field
LF1	—	Linear Fresnel solar field of number 1
LF2	—	Linear Fresnel solar field of number 2
$\dot{m}$	—	Mass flow rate, kg/s
N	—	Number of project Life time
n	—	Number of effects
NGB	—	Natural gas boiler
$\dot{Q}$	—	Specific heat consumption, kJ/kg
$\dot{Q}_{absorbed}$	—	Absorbed solar energy, W/m2
$\dot{Q}_{hl\_HTF}$	—	Heat transfer fluid heat loss, W/m2
$\dot{Q}_{hl_{piping}}$	—	Heat lost from solar field pipes, W/m2
$\dot{Q}_{LFR}$	—	Solar field useful thermal output, W/m2
SRC	—	Solar Rankine cycle
SORC	—	Solar organic Rankine cycle
T_{amb}	—	Ambient temperature, °C
TAWP	—	Total annual water production, m3/year
TAEG	—	Total annual electricity generation, kWh/year
TES	—	Thermal energy storage
TVC	—	Thermal vapor compression
T_{in}	—	Temperature of the heat transfer fluid at the inlet, °C

Greek symbols

η_{opt}	—	Optical efficiency
$\eta_{endloss}$	—	End loss efficiency
θ_i	—	Angle of incidence, degree

References

[1] Y. Yang, N. Lior, Performance analysis of combined humidified gas turbine power generation and multi-effect thermal vapor compression desalination systems part1: the desalination unit and its combination with a steam-injected gas turbine power system, Desalination, 196 (2006) 84–104.

[2] J.H. Reif, W. Alhalabi, Solar-thermal powered desalination: its significant challenges and potential. Renew. Sustain. Energy Rev., 48 (2015) 152–165.

[3] M. Agustín. T. Delgado, G.R. Lourdes, Preliminary design of seawater and brackish water reverse osmosis desalination systems driven by low-temperature solar organic Rankine cycles (SORC). Energy Convers. Manage., 51 (2010) 2913–2920.

[4] M. Agustín. T. Delgado, G.R. Lourdes, Analysis and optimization of the low-temperature solar organic Rankine cycle (ORC), Energy Convers. Manage., 51 (2010) 2846–2856.

[5] J. Wang, Zh. Yan, P. Zhao, Y. Dai, Off-design performance analysis of a solar-powered organic Rankine cycle, Energy Convers. Manage., 80 (2014) 150–157.

[6] L. Qoaider, A. Liqreina, Optimization of dry cooled parabolic trough (CSP) plants for the desert regions of the Middle East and North Africa (MENA), Solar Energy, 122 (2015) 976–985.

[7] C. Parrado, A. Girard, F. Simon, E. Fuentealba, 2050 LCOE (Levelized Cost of Energy) projection for a hybrid PV (photovoltaic)-CSP (concentrated solar power) plant in the Atacama Desert, Chile, Energy, 94 (2016) 422–430.

[8] E.R. Shouman, N.M. Khattab, Future economic of concentrating solar power (CSP) for electricity generation in Egypt, Renew. Sustain. Energy Rev., 41 (2015) 1119–1127.

[9] D. Cocco, G. Cau, Energy and economic analysis of concentrating solar power plants based on parabolic trough and linear Fresnel collectors, J. Power Energy, 229 (2015) 677–688.

[10] M. Balghouthi, S. Trabelsi, M. BenAmara, A. BelHadjAli, A. Guizani, Potential of concentrating solar power (CSP) technology in Tunisia and the possibility of interconnection with Europe, Renew. Sustain. Energy Rev., 46 (2016) 1227–1248.

[11] B.J. Alqahtani, D.P. Echeverri, Integrated solar combined cycle power plants: paving the way for thermal solar, Appl. Energy, 169 (2016) 927–936.

[12] Y. Li, Y. Yang, Thermodynamic analysis of a novel integrated solar combined cycle, Appl. Energy, 122 (2014) 133–142.

[13] G. Franchini, A. Perdichizzi, S. Ravelli, G. Barigozzi, A comparative study between parabolic trough and solar tower technologies in solar Rankine cycle and integrated solar combined cycle plants, Solar Energy, 98 (2013) 302–314.

[14] G. Manente, High performance integrated solar combined cycles with minimum modifications to the combined cycle power plant design, Energy Convers. Manage., 111 (2016) 186–197.

[15] G.C. Bakos, D. Parsa, Technoeconomic assessment of an integrated solar combined cycle power plant in Greece using line-focus parabolic trough collectors, Renew. Energy, 60 (2013) 598–603.

[16] E.M.A. Mokheimer, Y.N. Dabwan, M.A. Habib, S.A.M. Said, F.A. Al-Sulaiman, Development and assessment of integrating parabolic trough collectors with steam generation side of gas turbine cogeneration systems in Saudi Arabia, Appl. Energy, 141 (2015) 131–142.

[17] E.M.A. Mokheimer, Y.N. Dabwan, M.A. Habib, Optimal integration of solar energy with fossil fuel gas turbine cogeneration plants using three different CSP technologies in Saudi Arabia, Appl. Energy, 185 (2017) 1268–1280.

[18] A. Rovira, R. Barbero, M.J. Montes, R. Abbas, F. Varela, Analysis and comparison of integrated solar combined cycles using parabolic troughs and linear Fresnel reflectors as concentrating systems, Appl. Energy, 162 (2016) 990–1000.

[19] Fichtner (Fichtner GmbH & Co. KG) and DLR (Deutsches Zentrum für Luft und Raumfahrt e.V.), MENA Regional Water Outlook, Part II, Desalination Using Renewable Energy, Task 1–Desalination Potential; Task 2–Energy Requirements; Task 3–Concentrate Management. 2011. Available at: http://www.dlr.de/tt/Portaldata/41/Resources/dokumente/institut/system/projects/MENA_REGIONAL_WATER_OUTLOOK.pdf.
[20] B. Ortega-Delgado, L. García-Rodríguez, D.C. Alarcón-Padilla, Thermo economic comparison of integrating seawater desalination processes in a concentrating solar power plant of 5 MWe, Desalination, 392 (2016) 102–117.
[21] G. Fiorenza, V.K. Sharma, G. Braccio, Techno-economic evaluation of a solar powered water desalination plant, Energy Convers. Manage., 44 (2003) 2217–2240.
[22] P. Palenzuela, G. Zaragoza, D. Alarcón-Padilla, E. Guillén, M. Ibarra, J. Blanco, Assessment of different configurations for combined parabolic-trough (PT) solar power and desalination plants in arid regions, Energy, 36 (2011) 4950–4958.
[23] K.H.M. Bataineh, Multi-effect desalination plant combined with thermal compressor driven by steam generated by solar energy, Desalination, 385 (2016) 39–52.
[24] M.A. Sharaf, A.S. Nafey, L. García-Rodríguez, Thermo-economic analysis of solar thermal power cycles assisted MED-VC (multi effect distillation-vapor compression) desalination processes, Energy, 36 (2011) 2753–2764.
[25] B. Ortega-Delgado, P. Palenzuela, D.C. Alarcón-Padilla, Parametric study of a multi-effect distillation plant with thermal vapor compression for its integration into a Rankine cycle power block, Desalination, 394 (2016) 18–29.
[26] M. Moser, F. Trieb, T. Fichter, J. Kern, D. Hess, A flexible techno-economic model for the assessment of desalination plants driven by renewable energies, Desal. Wat. Treat., 55 (2014) 3091–3105.
[27] A. Kouta, F. Al-Sulaima, M. Atif, S.B. Marshad, Entropy, exergy, and cost analyses of solar driven cogeneration systems using supercritical CO_2 Brayton cycles and MEE-TVC desalination system, Energy Convers. Manage., 115 (2016) 253–264.
[28] G. Iaquaniello, A. Salladini, A. Mari, A.A. Mabrouk, H.E.S. Fath, Concentrating solar power (CSP) system integrated with MED–RO hybrid desalination, Desalination, 336 (2014) 121–128.
[29] F. Calise, M.D. Accadia, A. Macaluso, A. Piacentino, L. Vanoli, Exergetic and exergoeconomic analysis of a novel hybrid solar–geothermal polygeneration system producing energy and water, Energy Convers. Manage., 115 (2016) 200–220.
[30] M.A. Sharaf, A.S. Nafey, L. García-Rodríguez, Exergy and thermo-economic analyses of a combined solar organic cycle with multi effect distillation (MED) desalination process, Desalination, 272 (2011) 135–147.
[31] I. Baniasad Askari, M. Ameri, Techno economic feasibility analysis of Linear Fresnel solar field as thermal source of the MED/TVC desalination system, Desalination, 394 (2016) 1–17.
[32] R. Abbas, M.J. Montes, M. Piera, J.M. Martínez-Val, Solar radiation concentration features in linear Fresnel reflector arrays, Energy Convers. Manage., 54 (2012) 133–144.
[33] R. Abbas, M.J. Montes, M. Piera, J.M. Martínez-Val, High concentration linear Fresnel reflectors, Energy Convers. Manage., 72 (2013) 60–68.
[34] R. Gabbrielli, P. Castrataro, F. del Medico, M. di Palo, B. Lenzo, Levelized cost of heat for linear Fresnel concentrated solar systems, Energy Procedia, 49 (2014) 1340–1349.
[35] Y. Qiu, Y.L. He, Z.D. Cheng, K. Wang, Study on optical and thermal performance of a linear Fresnel solar reflector using molten salt as HTF with MCRT and FVM methods, Appl. Energy, 146 (2015) 162–173.
[36] http://www.irimo.ir/eng/wd/704-Stations-Network-and-Technical-Deputy.html.
[37] https://sam.nrel.gov/weather.
[38] http://www.dlr.de/tt/desktopdefault.aspx/tabid-2885/4422_read-16596.
[39] A. Giostri, M. Binotti, P. Silva, E. Macchi, G. Manzolini, Comparison of two linear collectors in solar thermal plants: parabolic trough versus Fresnel, J. Solar Energy Eng., 135 (2011) 621–630.
[40] B. Kelly, D. Kearney, Parabolic Trough Solar System Piping Model Final Report, National Renewable Energy Laboratory Subcontract Report NREL/SR-550-40165, 2006. Available at: http://www.nrel.gov/csp/troughnet/pdfs/40165.pdf.
[41] System Adviser Model (SAM), Version 2015.6.30. Available at: https://www.nrel.gov/analysis/sam/help/html-php/index.html?linear_fresnel_system_costs.htm.
[42] S. Loutatidou, H.A. Arafat, Techno-economic analysis of MED and RO desalination powered by low-enthalpy geothermal energy, Desalination, 365 (2015) 277–292.
[43] F. Verdier, R. Baten, Fichtner GmbH & Co.·KG, Bridging the Water Demand Gap: Desalination Consultative Workshop on Desalination and Renewable Energy, Muscat, Oman, 22–23 February, 2011.